



# Modeling biogeochemical dynamics in porous media: Practical considerations of pore scale variability, reaction networks, and microbial population dynamics in a sandy aquifer

E.L. King<sup>a</sup>, K. Tuncay<sup>b</sup>, P. Ortoleva<sup>c</sup>, C. Meile<sup>a,\*</sup>

<sup>a</sup> Department of Marine Sciences, University of Georgia, Athens GA 30602, USA

<sup>b</sup> Department of Civil Engineering, Middle East Technical University NCC, Kalkanli, Guzelyurt, TRNC, Mersin 10, Turkey

<sup>c</sup> Department of Chemistry, Indiana University Bloomington, Bloomington IN 47405, USA

## ARTICLE INFO

### Article history:

Received 3 January 2009

Received in revised form 9 October 2009

Accepted 10 December 2009

Available online 21 December 2009

### Keywords:

Reactive transport modeling

Pore scale heterogeneity

Biogeochemical reaction networks

Microbial population dynamics

## ABSTRACT

Prediction of the fate and environmental impacts of groundwater contaminants requires the identification of relevant biogeochemical processes and necessitates the macroscopic representation of microbial activity occurring at the microscale. Using a well-studied sandy aquifer environment, we evaluate the importance of pore distribution on organic matter respiration in a porous medium environment by performing spatially explicit simulations of microbial metabolism at the sub-millimeter scale. Model results using an idealized porous medium under non-biofilm forming conditions indicate that while some heterogeneity is observed for flow rates, distributions of microbes and dissolved organic substrates remain relatively homogenous at the grain scale. At the macroscale in the same environment, we assess the impact of a comprehensive reaction network description for a phenolic contaminant plume, and compare the findings to a setting describing organic matter breakdown in a coastal marine sediment. This comparison reveals the importance of reactions recycling reduced metabolites at redox interfaces, leading to a competition for oxidants. When the spatio-temporal dynamics of microbial groups are accounted for, our simulations show the importance of reaction energetics and nutrient limitations such as microbial nitrogen demands.

© 2009 Elsevier B.V. All rights reserved.

## 1. Introduction

To assess the persistence and fate of nutrients, contaminants, and pathogens in aquifers, it is necessary to understand their biogeochemical and transport behavior. Their spatio-temporal distribution depends on sorption and transport characteristics and chemical transformations, many of which are microbially mediated. Challenged by sparse observational data in subsurface environments, predictions of the fate of these substances typically rely on computational approaches. Models that couple transport processes with reactions result in tight interactions

between a multitude of chemical species. They are commonly used to quantitatively assess biogeochemical dynamics in aquifers and have provided significant insight into contaminant transport and decision making support (e.g. Cygan et al., 2007). While a comprehensive treatment of reactive transport relies on conservation of mass, momentum, and energy (Steeffel et al., 2005), in practice most models are based only on mass balance equations. For a single fluid phase, the governing equations for the various constituents are of the form (e.g. Miller et al., 1998):

$$\frac{\partial}{\partial t}(\theta\rho c_i) = -\nabla \cdot (j + v\theta\rho c_i) + \sum R \quad (1)$$

where  $\theta$  is fluid volume fraction,  $\rho$  is density,  $c_i$  is mass fraction of entity  $i$ ,  $\mathbf{v}$  is the advection velocity vector,  $\sum R$  is the net impact

\* Corresponding author. Department of Marine Sciences, University of Georgia, Athens GA 30602–3636, USA. Tel.: +1 706 542 6549; fax: +1 706 542 5888.

E-mail address: [cmeile@uga.edu](mailto:cmeile@uga.edu) (C. Meile).

of reactions  $R$ , and  $j$  denotes non-advective transport fluxes, which are typically described as a diffusive term with a diffusion tensor  $\mathbf{D}$  so that  $j = -\theta\rho\mathbf{D}\nabla c$ .

Some features in such reactive transport models can pose limits to their applicability. First, they rely on bulk properties that are averages over a representative elementary volume (REV; Zhang et al., 2000). In porous media, REVs must encompass several grains, implying that heterogeneity below that scale can be properly parameterized or has a negligible impact on reaction rate estimates (e.g. Szecsody et al., 1998; Wood et al., 2007). Second, description of transport processes via the use of a diffusion tensor assumes that non-Fickian transport is of minor importance (Hassanizadeh, 1995; Levy and Berkowitz, 2003). Third, use of Eq. (1) implies that the reaction network can be identified and parameterized. In order to do so, a finite set of reactions needs to be selected to represent a system of tremendous natural complexity, involving not only transformations in solution, surface catalysis, and precipitation and dissolution of mineral phases, but also the activity and dynamics of microbial populations. Volumetric reaction rates vary with abundance, distribution, metabolic capability, and cell-specific activity of microbial populations. The microbial community has the potential to both modify and adjust to environmental conditions through changes in community composition, alterations of activity levels, chemotactic movement and metabolic plasticity (e.g. Ginn et al., 2002; Pett-Ridge and Firestone, 2005).

Due to the central role of organics as energy sources for subsurface microbial life and the importance of redox conditions for the fate of contaminants, many studies of elemental cycling in porous media either focus directly or indirectly on the breakdown of organic compounds and the associated use of electron acceptors. Organic matter mineralization can be conceptualized as fermentation and hydrolysis of high molecular weight compounds producing low molecular weight substances such as acetate and other volatile fatty acids as well as  $\text{H}_2$ , which then get respired through terminal metabolism, consuming electron acceptors such as  $\text{O}_2$ , nitrate, metal oxides and sulfate (Lovley and Goodwin, 1988; Jakobsen et al., 1998). The evolution of reactive transport modeling to elucidate the dynamics of elemental cycling has involved an increase in the complexity of the reactions. For example, McNab and Narasimhan (1994, 1995) developed a model to simulate the attenuation and breakdown of petroleum hydrocarbons in an aquifer, employing a partial equilibrium approach, while Jakobsen and Postma (1999) used this approach to study iron oxide reduction, sulfate reduction, and methanogenesis in a shallow aquifer. Mayer et al. (2001) presented a fully kinetic model to describe contaminant dynamics along flow lines in a contaminant plume over an ~50 year period utilizing reactions involved in the degradation of phenol coupled to terminal electron accepting processes. Emphasizing the importance of a comprehensive reaction network, Hunter et al. (1998) developed a fully kinetic model that included mineral precipitation and a suite of secondary reactions describing the reoxidation of reduced metabolites produced in the breakdown of organic matter in an aquifer, similar to the work of Boudreau (1996), Soetaert et al. (1996), and Van Cappellen and Wang (1996) on early diagenesis in marine sediments. Recent studies have also taken into account thermodynamic constraints on both abiotic and microbially mediated reactions or focused on improving representations of microbial activity. For example, Jakobsen

and Cold (2007) implemented energy constraints on reactions in a sandy aquifer while Jin and Bethke (2003), based on the work of Boudart (1976), developed a reaction rate expression which accounts for the energy available in the microbe's environment through a dependency on the Gibbs free energy of reaction. The effect of microniches – i.e. scales typically not resolved explicitly – on redox processes has been investigated (e.g., Jakobsen, 2007; Sochaczewski et al. 2008), and numerous studies have quantified the effect of pore scale substrate heterogeneity on reaction rates in reactive flows in soil columns (e.g., Raje and Kapoor, 2000; Gramling et al., 2002), at stationary reaction fronts (e.g., Meile and Tuncay, 2006), or on mineral dissolution under a variety of environmental conditions (e.g., Li et al., 2006, 2008).

In this study we assess the impact of three factors that may limit the applicability of reactive transport models in low-temperature subsurface environments: (i) pore scale heterogeneity in substrate distribution and its effect on microbial processes, (ii) impact of the scope of the reaction network considered on predicted metabolite distributions and process dynamics, and (iii) role of constraints on microbial population dynamics. We address these issues in the setting of a sandstone aquifer (Sherwood aquifer, West Midlands, UK) with a phenolic contaminant plume that has been documented extensively in the literature (Thornton et al., 2001a,b; Mayer et al., 2001; Watson et al., 2005). First, we focus on flow fields and substrate availability at the grain scale. Simulations of flow and reaction are performed in a two-dimensional representation of a porous medium taken from the Sherwood aquifer to assess if pore scale heterogeneity in substrate and biomass distributions is likely to occur under conditions that are representative for the metabolism of dissolved organic matter. Second, macroscopic reaction transport simulations are performed that extend the work of Watson et al. (2005), who modeled the contaminants originating from a coal tar distillation plant which have been penetrating into the aquifer since the early 1950s. The effect of the comprehensiveness of the reaction network is evaluated by assessing the impact of additional reoxidation reactions and mineral precipitation. The findings are then compared to the roles of these additional reactions in early diagenesis in a coastal marine sediment. Controls on microbial populations and their interactions with the geochemical environment are considered by integration of explicit descriptions of functional microbial groups into reactive transport models.

## 2. Methods and applications

### 2.1. Pore scale model

To investigate the interplay between transport of chemicals and microbial dynamics, simulations at the pore scale are performed. The flow field is required in the mass conservation equations for chemical and biological constituents and is solved using the incompressible Navier–Stokes equations:

$$\begin{aligned} \rho \frac{\partial \mathbf{u}}{\partial t} - \eta \nabla^2 \mathbf{u} + \rho(\mathbf{u} \cdot \nabla) \mathbf{u} + \nabla p &= 0 \\ \nabla \cdot \mathbf{u} &= 0 \end{aligned} \quad (2)$$

where  $\rho$  is fluid density ( $1000 \text{ kg m}^{-3}$ ),  $\mathbf{u}$  is the velocity vector,  $p$  is pressure, and  $\eta$  is the dynamic viscosity ( $0.001 \text{ Pa s}$ ). The

domain is derived from a 2D image of a porous medium depicting grains and pore space (see below) and is established by flipping the image horizontally and/or vertically. The resulting four components are joined together so that the pore structures match up at all boundaries. Fluid flow is produced by an imposed horizontal macroscopic pressure gradient, and no flow conditions are imposed at grain surfaces. Periodic boundary conditions for flow velocities are imposed between the left (inflow) and right (outflow) sides and the top and bottom of the domain (in Fig. 1).

The biogeochemistry considered is simplified and is represented by concentrations of acetate ( $C$ ) and biomass in solution ( $B$ ) and on the grain surfaces ( $B_{sfc}$ , expressed per area) only. The governing equations take into account advection, diffusion and reaction:

$$\frac{\partial C}{\partial t} = \nabla \cdot (D_C \nabla C) - \mathbf{u} \cdot \nabla C - R_{ac} B + R_{prod} \quad (3)$$

$$\frac{\partial B}{\partial t} = \nabla \cdot (D_B \nabla B) - \mathbf{u} \cdot \nabla B + g R_{ac} B - \mu_B B \quad (4)$$

$$\frac{\partial B_{sfc}}{\partial t} = g R_{ac} B_{sfc} - \mu_B B_{sfc} + R_{ex} \quad (5)$$

where  $D_C$  and  $D_B$  are the diffusion coefficients for acetate and biomass in solution,  $R_{prod}$  is the volumetric acetate production rate through fermentation,  $R_{ac}$  is the cell-specific rate of acetate consumption,  $g$  is the growth efficiency,  $R_{ex}$  is the net exchange rate due to adsorption and desorption of bacteria to and from grain surfaces (see Eq. (6) below), and  $\mu_B$  describes the rate of cell death (see next paragraph). Acetate uptake by surface attached bacteria is accounted for via a flux condition at the grain surface,  $\mathbf{n} \cdot (-D_C \nabla C + \mathbf{u} C) = -R_{ac} B_{sfc}$ , where  $\mathbf{n}$  is the outward normal vector to the grain surface. Continuity across connected interfaces is ensured. Boundary conditions for biomass concentrations are established in the same fashion, except that at the grain surface, the flux is set equal to the net rate of attachment and detachment ( $R_{ex}$ ), i.e.  $\mathbf{n} \cdot (-D_B \nabla B + \mathbf{u} B) = R_{ex}$ . Two-dimensional representations of grain geometries are implemented in the finite element simulation environment COMSOL. Pore space is discretized into

~135,000 triangular finite elements. Fluid flow is computed using a direct solver (UMFPACK). Subsequently, steady state distributions of the remaining state variables ( $C$ ,  $B$ ,  $B_{sfc}$ ) are solved for using constant initial conditions ( $1 \times 10^{-4}$  M acetate; 0.04 grams dry weight ( $g_{dw}$ )  $m^{-3}$  biomass) and employing UMFPACK.

Pore scale simulations are performed for a grain arrangement from the Sherwood sandstone aquifer using an image from Scott and Barker (2005) of size 2.3 by 1.76 mm. Porosity ( $\theta$ ) is 0.44, and the pore volume to grain surface area  $s_{VA}$  is approximately  $5.4 \times 10^{-5}$  m. The macroscopic pressure gradients are chosen so that mean flow velocities computed are consistent with that seen in the phenol contaminant plume (Watson et al., 2005), on the order of  $2 \times 10^{-7}$  m  $s^{-1}$ . The diffusion coefficient for acetate is set to  $10^{-9}$  m<sup>2</sup>  $s^{-1}$  (Boudreau, 1996) and for biomass is set to  $10^{-10}$  m<sup>2</sup>  $s^{-1}$ . Acetate production is set to  $R_{prod} = 10^{-8}$  mol  $m^{-3}$   $s^{-1}$  to be consistent with phenol breakdown rates seen in Watson et al. (2005), and is distributed evenly throughout the domain. Acetate consumption is defined using Monod kinetics,  $R_{ac} = k_{ac} \frac{C}{K_{mac} + C}$ , with the half saturation constant  $K_{mac}$  set to 10  $\mu$ M and a maximum rate  $k_{ac} = 20$  mmol  $g_{dw}^{-1}$   $hr^{-1}$  (Esteve-Núñez et al., 2005). The growth efficiency,  $g$  (Eq. (5)), is defined as a function of the acetate concentration based on cell model results and reaches about 4.4  $g_{dw}$   $mol_{acetate}^{-1}$  under replete substrate conditions and approaches 0 at approximately 0.5  $\mu$ M acetate levels (King et al., 2009). Acetate concentrations below this threshold are not sufficient to sustain growth as cell maintenance requirements exceed ATP production (King et al., 2009), and cell death occurs at a rate of 1% of the maximum growth rate. Following Murphy and Ginn (2000) and Sakers and Hornberger (1996), microbial surface attachment and detachment ( $R_{ex}$ ) are given by:

$$R_{ex} = \frac{k_{ads} (\Gamma_{max} - B_{sfc})}{s_{VA} \Gamma_{max}} B - k_{des} B_{sfc} \quad (6)$$

where  $\Gamma_{max}$  is the maximum surface coverage of microbes on the grains ( $0.04$   $g_{dw} m^{-2}$ ) calculated from monolayer coverage assuming a rectangular bacterial shape of size  $0.4 \mu m \times 2.5 \mu m$  (Seeliger et al., 1998) and a cell dry weight of 40 fg,  $k_{ads}$  is the cell surface attachment rate of  $2.1 \times 10^{-3}$   $s^{-1}$ , and  $k_{des}$  is the

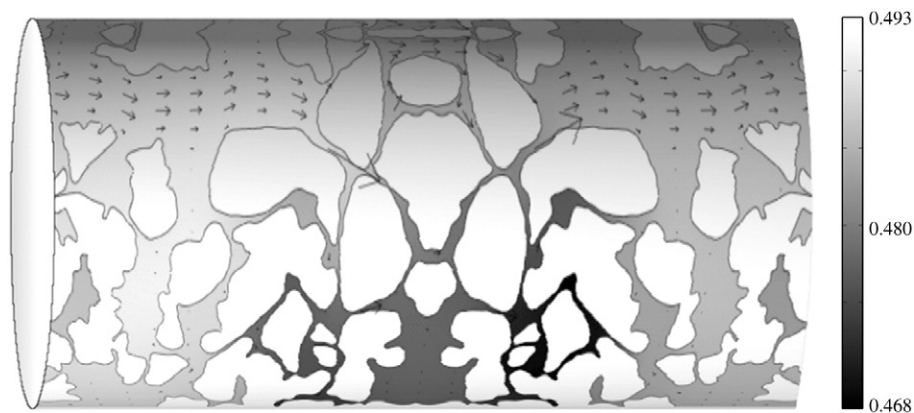


Fig. 1. Porous media represented as a cylinder by folding the top and bottom of the domain together. Modeled acetate concentration in the pore scale simulation ( $\mu$ M) is depicted in the shaded regions. Arrows represent fluid flow with arrow size proportional to the velocity in the pores.

cell surface detachment rate of  $1.2 \times 10^{-5} \text{ s}^{-1}$  (Bradford et al., 2002). This simplified representation limits surface attached bacteria to a monolayer with no significant feedback on fluid flow. Hence, it cannot represent the formation of biofilms that can lead to heterogeneity at the pore scale (e.g. Davison et al., 1997; Suchomel et al., 1998). Also, while there is no independent observation validating the flow field, by computing hydraulic conductivity from pore scale simulations and comparing them to experimentally determined values in larger scale experiments, Narsilio et al. (2009) showed the validity of Navier–Stokes pore scale simulations in a comparable setting. Finally, our pore scale model does not account for bimodal porosity distributions, which have been shown to lead to preferential flow paths that can result in patchy distributions of substrate and biomass at the cm scale (Coppola et al., 2009). This is juxtaposed by considering only two rather than the physical three spatial dimensions, which tends to underestimate the connectivity of the pore network and hence promote patchy distributions.

## 2.2. Large scale models

The macroscale reactive transport simulations are based on the work by Watson et al. (2005) who studied the fate of a contaminant plume using a 2D vertical aquifer cross section. Their description included phenol breakdown as a two-step process. The first step involved fermentative reactions producing acetate, inorganic carbon, and  $\text{H}_2$  and the second step considered the subsequent breakdown of these intermediates. The reaction network also included sorption reactions involving iron phases and took into account the precipitation of iron sulfides. In our approach, we adapted the reactive transport model presented in Spiteri et al. (2008) to simulate the spatio-temporal evolution of this phenol plume. In brief, based on conservation of mass, the concentration field of a solute ( $C_k$ , in mass per pore volume) is given by

$$\frac{\partial \theta C_k}{\partial t} = \nabla \cdot (\mathbf{D}^* \nabla C_k) - \nabla \cdot (\theta \mathbf{v} C_k) + \theta R_k \quad (7)$$

where  $\theta$  is porosity,  $\mathbf{v}$  is the flow velocity, and  $R_k$  is the net reaction rate of species  $k$  in mass per time and pore volume. The diffusion–dispersion tensor  $\mathbf{D}^*$  is defined as

$$\mathbf{D}_{ij}^* = \theta D^m \delta_{ij} + (\alpha_L - \alpha_T) \frac{v_i v_j}{|v|} + \alpha_T |v| \delta_{ij}, \quad (8)$$

where  $D^m$ ,  $\delta_{ij}$ ,  $\alpha_L$  and  $\alpha_T$  are tortuosity corrected *in situ* molecular diffusion coefficient, Kronecker symbol, and longitudinal and transverse dispersivities, respectively (Scheidegger, 1961). Solids and surface attached microorganisms are assumed to be immobile, so that

$$\frac{d(1-\theta)c_k}{dt} = (1-\theta)r_k \quad (9)$$

where  $c_k$  is the concentration of compound  $k$  in mass per solid volume, and  $r_k$  is the net reaction rate of species  $k$  in mass per time and solid volume.

The governing equations are discretized using a Galerkin finite element formulation and forward Euler time stepping.

Transport and reaction operators are split (Steeffel and MacQuarrie, 1996) and in each timestep, the transport of the solutes is first computed using a diagonally preconditioned conjugate gradient solver (Reddy, 1993; Meile and Tuncay, 2006). Subsequently, the set of coupled ordinary differential equations representing the reaction network is solved at each node using the VODE solver, employing backward differentiation and full Jacobian settings (Brown et al., 1989).

Equilibrium reactions describing the speciation and surface adsorption of reactants are computed at the end of each timestep through mass-action expressions that are simplifications of these complex reactions. Mass action is expressed as  $a_j = K_j \prod_i a_i^{q_{ji}}$ , where  $a$  denote activities,  $K_j$  is the equilibrium constant,  $q_{ji}$  are the stoichiometric coefficients and  $nc$  is the number of components. Mass conservation is ensured (to within a tolerance of  $1 \times 10^{-10} \text{ mol m}^{-3}$ ) by matching the total imposed mass of a component  $i$  ( $T_i$ ) with the summed contributions from all species ( $S$ ) in which that element is speciated,  $T_i = \sum_j q_{ji}[S_j]$ , where  $m$  is the number of species. Activities and concentrations are linked via activity coefficients assuming an ionic strength of 0.1 and computed using the Davies equations. Mass-action laws are linearized by a log transformation, and the system  $a_i \leftarrow a_i - \mathbf{J}^{-1} Y_i$ , where  $Y_i = T_i - \sum_j q_{ji}[S_j]$  and  $\mathbf{J}$  denotes the Jacobian matrix  $J_{ij} = \frac{\partial Y_i}{\partial a_j}$ , is solved iteratively using a Newton–Raphson root finding procedure (Tadanier and Eick, 2002). In this manner, pH is computed at each timestep from the local solution composition, taking into account the acid–base equilibrium of the dissolved inorganic carbon and sulfide species, precipitation and dissolution of iron sulfides, as well as fast surface exchange reactions.

Simulations are performed at a well-characterized site contaminated with phenolic compounds in the English West Midlands (e.g. Thornton et al., 2001a,b; Mayer et al., 2001), with a uniform horizontal plume propagation speed ( $v_i$ ) on the order of  $10 \text{ m yr}^{-1}$ . We compare simulations for a number of reaction networks that differ in their complexity, ranging from a set that only includes the oxidation of high molecular weight organic matter and subsequent terminal metabolism to a description that encompasses chemotrophic and abiotic oxidation reactions that compete with the heterotrophic respiration for electron acceptors, precipitation reactions and microbial dynamics. The baseline reaction network for the contaminant plume simulations follows Watson et al. (2005), with the exception that their work employs different  $k_{\text{max}}$  values inside and outside of the plume while we employ one single value for each reaction. The baseline network considers the fermentation of phenol, and the subsequent respiration of  $\text{H}_2$ , precipitation of iron sulfides, as well as sorption reactions involving iron phases (“baseline” network, consisting of primary (P) and equilibrium (E) reactions given in Table 1). The complexity of the “baseline” network is increased by including the oxidation of reduced species (secondary reactions (S) in Table 1) and further expanded by taking carbonate mineral precipitation and dissolution reactions into account (mineral reactions (M) in Table 1). Parameters for secondary reactions were taken from Hunter et al. (1998), except that the rate constants for iron oxidation with  $\text{O}_2$  and methane oxidation with sulfate

**Table 1**  
Reactions.

Reactions	Stoichiometry	Rate law ( $F_{kin}$ ) <sup>a</sup>	#
<i>Primary reactions (P)</i> <sup>b</sup>			
Aerobic degradation	$C_6H_5OH + 7O_2 + 3H_2O \rightarrow 6HCO_3^- + 6H^+$	$k_{maxP1} \cdot M_{1,phenol} \cdot M_{1,O2}$	P1
Denitrification	$C_6H_5OH + 5.6NO_3^- + 0.2H_2O \rightarrow 6HCO_3^- + 0.4H^+ + 2.8N_2$	$k_{maxP2} \cdot M_{2,phenol} \cdot M_{2,NO3} \cdot I_{2,O2}$	P2
Fermentation	$C_6H_5OH + 5H_2O \rightarrow 3CH_3COOH + 2H_2$	$k_{maxP3} \cdot M_{3,phenol} \cdot I_{3,O2} \cdot I_{3,NO3} \cdot I_{3,phenol}$	P3
Fermentation	$C_6H_5OH + 17H_2O \rightarrow 6HCO_3^- + 6H^+ + 14H_2$	$k_{maxP4} \cdot M_{4,phenol} \cdot I_{4,O2} \cdot I_{4,NO3} \cdot I_{4,phenol}$	P4
Manganese reduction	$H_2 + MnO_2 + 2H^+ \rightarrow 2H_2O + Mn^{2+}$	$k_{maxP5} \cdot M_{5,H2} \cdot I_{5,O2} \cdot I_{5,NO3} \cdot I_{5,phenol}$	P5
Iron reduction	$H_2 + 2FeOOH + 4H^+ \rightarrow 4H_2O + 2Fe^{2+}$	$k_{maxP6} \cdot M_{6,H2} \cdot I_{6,O2} \cdot I_{6,NO3} \cdot I_{6,phenol}$	P6
Sulfate reduction	$H_2 + 0.25SO_4^{2-} + 0.25H^+ \rightarrow H_2O + 0.25HS^-$	$k_{maxP7} \cdot M_{7,H2} \cdot M_{7,SO4} \cdot I_{7,O2} \cdot I_{7,NO3} \cdot I_{7,phenol}$	P7
Methanogenesis	$H_2 + 0.25HCO_3^- + 0.25H^+ \rightarrow 0.75H_2O + 0.25CH_4$	$k_{maxP8} \cdot M_{8,H2} \cdot I_{8,O2} \cdot I_{8,NO3} \cdot I_{8,phenol}$	P8
<i>Secondary reactions (S)</i>			
Manganese oxidation	$Mn^{2+} + 0.5O_2 + H_2O \rightarrow MnO_2 + 2H^+$	$k_{maxS1} \cdot [Mn^{2+}] \cdot [O_2]$	S1
Iron oxidation	$Fe^{2+} + 0.25O_2 + 1.5H_2O \rightarrow FeOOH + 2H^+$	$k_{maxS2} \cdot [Fe^{2+}] \cdot [O_2]$	S2
Iron oxidation by MnO <sub>2</sub>	$2Fe^{2+} + MnO_2 + 2H_2O \rightarrow 2FeOOH + Mn^{2+} + 2H^+$	$k_{maxS3} \cdot [Fe^{2+}] \cdot [MnO_2]$	S3
Sulfide oxidation	$H_2S + 2O_2 \rightarrow SO_4^{2-} + 2H^+$	$k_{maxS4} \cdot [TS] \cdot [O_2]$	S4
Sulfide oxidation by MnO <sub>2</sub>	$H_2S + MnO_2 + 2H^+ \rightarrow Mn^{2+} + S^0 + 2H_2O$	$k_{maxS5} \cdot [TS] \cdot [MnO_2]$	S5
Sulfide ox. via FeOOH	$H_2S + 2FeOOH + 4H^+ \rightarrow 2Fe^{2+} + S^0 + 4H_2O$	$k_{maxS6} \cdot [TS] \cdot [FeOOH]$	S6
FeS oxidation	$FeS + 2O_2 \rightarrow Fe^{2+} + SO_4^{2-}$	$k_{maxS7} \cdot [FeS] \cdot [O_2]$	S7
Methane oxidation	$CH_4 + 2O_2 \rightarrow CO_2 + 2H_2O$	$k_{maxS8} \cdot [CH_4] \cdot [O_2]$	S8
Methane ox. with sulfate	$CH_4 + SO_4^{2-} + H^+ \rightarrow H_2S + HCO_3^- + H_2O$	$k_{maxS9} \cdot [CH_4] \cdot [SO_4^{2-}]$	S9
Nitrification	$NH_4^+ + 2O_2 \rightarrow NO_3^- + 2H^+ + H_2O$	$k_{maxS10} \cdot [NH_4^+] \cdot [O_2]$	S10
<i>Mineral dissolution/precipitation reactions (M)</i>			
MnCO <sub>3</sub> precip/dissolution	$Mn^{2+} + HCO_3^- \rightarrow MnCO_3 + H^+$	$(\delta_p \cdot k_{p,MnCO3} + \delta_d \cdot k_{d,MnCO3}) \cdot [MnCO_3] \cdot (\Omega_{MnCO3} - 1)$	M1
FeCO <sub>3</sub> precip/dissolution	$Fe^{2+} + HCO_3^- \rightarrow FeCO_3 + H^+$	$(\delta_p \cdot k_{p,FeCO3} + \delta_d \cdot k_{d,FeCO3}) \cdot [FeCO_3] \cdot (\Omega_{FeCO3} - 1)$	M2
<i>Equilibrium reactions (E)</i>			
> FeOH + Mn <sup>2+</sup> => FeOMn <sup>+</sup> + H <sup>+</sup>	E1	$HCO_3^- = H^+ + CO_3^{2-}$	E6
> FeOH + H <sup>+</sup> => FeOH <sub>2</sub>	E2	$H_2CO_3 = H^+ + HCO_3^-$	E7
> FeOH => FeO <sup>-</sup> + H <sup>+</sup>	E3	$H_2O = H^+ + OH^-$	E8
> FeOH + Fe <sup>2+</sup> => FeOFe <sup>+</sup> + H <sup>+</sup>	E4	$FeS + H^+ = Fe^{2+} + HS^-$	E9
> FeOH + Fe <sup>2+</sup> + H <sub>2</sub> O => FeOFeOH + 2H <sup>+</sup>	E5	$H_2S = HS^- + H^+$	E10

<sup>a</sup> Monod and inhibition terms are defined as  $M_{i,C} = [C]/(K_{m,i} + [C])$  and  $I_{j,C} = K_{i,j}/(K_{i,j} + [C])$ , respectively. Values for the reaction parameters are given in Table 2. For the mineral precipitation reactions/dissolution reactions,  $\delta_p = 1$  and  $\delta_d = 0$  if  $\Omega < 1$  and  $\delta_p = 0$  and  $\delta_d = 1$  if  $\Omega \geq 1$ . Saturation states  $\Omega_{XCO_3}$  are defined as  $[X^{2+}][HCO_3^-]/(K_{XCO_3}[H^+])$ , where  $X = Mn$  or  $Fe$ .

<sup>b</sup> In the “microbial” simulations, the kinetic expressions  $F_{kin}$  in P1–8 are divided by typical biomass concentrations,  $B^0$ , set to  $0.8 \text{ g}_{dw} \text{ m}^{-3}$ . Phenol respiring organisms are responsible for reactions P1 and P2, phenol fermenters for P3 and P4, and H<sub>2</sub> utilizing organisms for P5–P8.

were modified to provide results that were consistent with the field data shown in Thornton et al. (2001b).

In the above formulations, the microbial populations are not represented explicitly, even though they catalyze the majority of the processes considered. To take into account microbial dynamics, “microbial” model simulations were performed that included three key functional groups of microbes that promote the breakdown of phenol and consumption of H<sub>2</sub> (phenol fermenting, phenol respiring, and H<sub>2</sub> respiring organisms; Table 1). The microbial groups are described by

$$\frac{\partial \theta B_i}{\partial t} = \nabla \cdot (\mathbf{D}^* \nabla B_i) - \nabla \cdot (\theta \mathbf{v} B_i) + \theta (g \delta R_i - \mu_i B_i) \quad (10)$$

where  $\mu_i$  is the death rate of microbial group  $i$  (Table 2) and  $\delta$  denotes the ammonium availability ( $\delta = 1$  if  $NH_4^+$  is present and 0 otherwise). Ammonium is subject to oxidation as well as biological uptake and recycling through cell death. Biological uptake of ammonium is dependent on cell growth by assuming a cell carbon content of  $0.22 \text{ g}_C \text{ ml}^{-1}$  (Bratbak and Dundas, 1984) and a Redfield C:N ratio. Upon death, ammonium is released from the cells in the same proportions as incorporated during growth. Ammonium was not accounted for in Watson

et al. (2005) and boundary conditions are implemented based upon well data (Williams et al., 2001). Reaction rates are formulated as in the simulations without microbial dynamics (i.e. the kinetic expressions  $F_{kin}$  given in Table 1) except that they also contain a dependency on thermodynamic conditions ( $F_{thd}$ ) and biomass abundance:

$$R_i = F_{kin} \cdot F_{thd} \cdot B \quad (11)$$

where  $B$  reflects the biomass concentration of the microbial population performing the reaction. The thermodynamic factor  $F_{thd}$  accounts for the energy available in the microbe's environment through a dependency on the Gibbs free energy of reaction (Boudart, 1976; Jin and Bethke, 2003), and reflects that catabolic processes will ultimately shut down under conditions that do not allow for ATP production. This factor is defined as  $\max \left[ 0, 1 - \exp \left( \frac{-\nabla G_{rxn} - m \nabla G_{ATP}}{\chi RT} \right) \right]$ , where  $\Delta G_{rxn}$  is the Gibbs free energy of reaction,  $\Delta G_{rxn}$  is the phosphorylation potential and  $m$  and  $\chi$  are reaction specific parameters (Jin and Bethke (2005); Table 2).

Additional simulations are performed at a coastal marine site (station S4) in the eastern Skagerrak between Denmark

**Table 2**

Model parameters (sources provided as leading superscripts).

Parameter	Value	Parameter	Value
<i>Rate constants</i>			
<sup>a</sup> k <sub>maxP1</sub>	4.00 × 10 <sup>-10</sup> mol L <sup>-1</sup> s <sup>-1</sup>	<sup>c</sup> k <sub>maxS2</sub>	3.17 × 10 <sup>-1</sup> L mol <sup>-1</sup> s <sup>-1</sup>
<sup>a</sup> k <sub>maxP2</sub>	4.00 × 10 <sup>-11</sup> mol L <sup>-1</sup> s <sup>-1</sup>	<sup>f</sup> k <sub>maxS3</sub>	3.17 × 10 <sup>-8</sup> L mol <sup>-1</sup> s <sup>-1</sup>
<sup>a</sup> k <sub>maxP3</sub>	8.40 × 10 <sup>-13</sup> mol L <sup>-1</sup> s <sup>-1</sup>	<sup>c</sup> k <sub>maxS4</sub>	5.07 × 10 <sup>-3</sup> L mol <sup>-1</sup> s <sup>-1</sup>
<sup>a</sup> k <sub>maxP4</sub>	2.30 × 10 <sup>-13</sup> mol L <sup>-1</sup> s <sup>-1</sup>	<sup>c</sup> k <sub>maxS5</sub>	6.34 × 10 <sup>-4</sup> L mol <sup>-1</sup> s <sup>-1</sup>
<sup>a</sup> k <sub>maxP5</sub>	9.80 × 10 <sup>-12</sup> mol L <sup>-1</sup> s <sup>-1</sup>	<sup>c</sup> k <sub>maxS6</sub>	2.54 × 10 <sup>-4</sup> L mol <sup>-1</sup> s <sup>-1</sup>
<sup>a</sup> k <sub>maxP6</sub>	2.20 × 10 <sup>-11</sup> mol L <sup>-1</sup> s <sup>-1</sup>	<sup>c</sup> k <sub>maxS7</sub>	9.51 × 10 <sup>-3</sup> L mol <sup>-1</sup> s <sup>-1</sup>
<sup>a</sup> k <sub>maxP7</sub>	8.40 × 10 <sup>-11</sup> mol L <sup>-1</sup> s <sup>-1</sup>	<sup>c</sup> k <sub>maxS8</sub>	3.17 × 10 <sup>2</sup> L mol <sup>-1</sup> s <sup>-1</sup>
<sup>a</sup> k <sub>maxP8</sub>	4.34 × 10 <sup>-10</sup> mol L <sup>-1</sup> s <sup>-1</sup>	<sup>f</sup> k <sub>maxS9</sub>	3.17 × 10 <sup>-7</sup> L mol <sup>-1</sup> s <sup>-1</sup>
<sup>c</sup> k <sub>maxS1</sub>	3.17 × 10 <sup>-1</sup> L mol <sup>-1</sup> s <sup>-1</sup>	<sup>c</sup> k <sub>maxS10</sub>	1.59 × 10 <sup>-1</sup> L mol <sup>-1</sup> s <sup>-1</sup>
<i>Monod and inhibition constants</i>			
<sup>a</sup> K <sub>m,1-4(phenol)</sub>	1.10 × 10 <sup>-4</sup> mol L <sup>-1</sup>	<sup>a</sup> K <sub>i,2(O2)</sub>	6.20 × 10 <sup>-6</sup> mol L <sup>-1</sup>
<sup>a</sup> K <sub>m,5-6(H2)</sub>	5.00 × 10 <sup>-7</sup> mol L <sup>-1</sup>	<sup>a</sup> K <sub>i,3-4(O2)</sub>	3.10 × 10 <sup>-5</sup> mol L <sup>-1</sup>
<sup>a</sup> K <sub>m,7(H2)</sub>	1.00 × 10 <sup>-6</sup> mol L <sup>-1</sup>	<sup>a</sup> K <sub>i,3-4(NO3)</sub>	1.60 × 10 <sup>-5</sup> mol L <sup>-1</sup>
<sup>a</sup> K <sub>m,8(H2)</sub>	5.00 × 10 <sup>-6</sup> mol L <sup>-1</sup>	<sup>a</sup> K <sub>i,3-4(phenol)</sub>	6.00 × 10 <sup>-2</sup> mol L <sup>-1</sup>
<sup>a</sup> K <sub>m,1(O2)</sub>	3.10 × 10 <sup>-6</sup> mol L <sup>-1</sup>	<sup>a</sup> K <sub>i,5-8(O2)</sub>	3.10 × 10 <sup>-5</sup> mol L <sup>-1</sup>
<sup>a</sup> K <sub>m,2(NO3)</sub>	8.10 × 10 <sup>-6</sup> mol L <sup>-1</sup>	<sup>a</sup> K <sub>i,5-8(NO3)</sub>	1.60 × 10 <sup>-5</sup> mol L <sup>-1</sup>
<sup>a</sup> K <sub>m,7(SO4)</sub>	1.60 × 10 <sup>-3</sup> mol L <sup>-1</sup>	<sup>a</sup> K <sub>i,5-8(phenol)</sub>	4.00 × 10 <sup>-2</sup> mol L <sup>-1</sup>
<i>Mineral reactions</i>			
<sup>c</sup> k <sub>p,MnCO3</sub>	3.17 × 10 <sup>-6</sup> mol dm <sup>-3</sup> s <sup>-1</sup>	<sup>c</sup> k <sub>p,FeCO3</sub>	1.59 × 10 <sup>-6</sup> mol dm <sup>-3</sup> s <sup>-1</sup>
<sup>c</sup> k <sub>d,MnCO3</sub>	3.17 × 10 <sup>-12</sup> s <sup>-1</sup>	<sup>c</sup> k <sub>d,FeCO3</sub>	1.59 × 10 <sup>-12</sup> s <sup>-1</sup>
<sup>b</sup> K <sub>MnCO3</sub>	0.8690	<sup>b</sup> K <sub>FeCO3</sub>	0.2748
<i>Microbial growth and thermodynamics</i>			
<sup>d</sup> χ <sub>1</sub>	56	<sup>d</sup> m <sub>5-6</sub>	2/3
<sup>d</sup> χ <sub>2</sub>	28	<sup>d</sup> m <sub>7</sub>	1/3
<sup>d</sup> χ <sub>3-8</sub>	2	<sup>d</sup> m <sub>8</sub>	2/9
<sup>d</sup> m <sub>1</sub>	28	<sup>d</sup> ΔG <sub>ATP</sub>	50 kJ mol <sup>-1</sup>
<sup>d</sup> m <sub>2</sub>	28/3	<sup>e</sup> μ <sub>1</sub>	3.3 × 10 <sup>-10</sup> s <sup>-1</sup>
<sup>d</sup> m <sub>3</sub>	2/3	<sup>e</sup> μ <sub>2</sub>	1.65 × 10 <sup>-11</sup> s <sup>-1</sup>
<sup>d</sup> m <sub>4</sub>	1	<sup>e</sup> μ <sub>3</sub>	7.01 × 10 <sup>-11</sup> s <sup>-1</sup>
<i>Transport parameters</i>			
<sup>a</sup> α <sub>t</sub>	1 m	<sup>d</sup> D <sup>m</sup>	10 <sup>-9</sup> m <sup>2</sup> s <sup>-1</sup>
<sup>a</sup> α <sub>r</sub>	4 × 10 <sup>-4</sup> m		

<sup>a</sup> Watson et al. (2005) (note that in contrast to Watson et al. (2005), no spatial variation in rate constants is considered here).

<sup>b</sup> Stumm and Morgan (1996).

<sup>c</sup> Hunter et al. (1998).

<sup>d</sup> Jin and Bethke (2005) — note that the values for *m* and *χ* given there have been adjusted for the number electrons transferred per reaction.

<sup>e</sup> Death rates are calculated as 1% of their respective maximum achieved growth rates.

<sup>f</sup> Inferred from simulations.

and Norway. The 1D reactive transport model STEADYSED, calibrated for this site (Wang and Van Cappellen, 1996), was employed to analyze the effects of using simplified reaction networks describing sedimentary early diagenesis. Similar to the contaminant plume setting, the model takes into account the decomposition of organic matter, which includes oxic respiration, denitrification, manganese and iron oxide reduction, sulfate reduction, and methanogenesis, but it does not explicitly account for the intermediates of terminal electron accepting processes (e.g. H<sub>2</sub> and acetate). Reduced species are subject to secondary redox reactions and to mineral precipitation and adsorption, leading to a reaction network similar to that considered in the contaminant plume simulations, not including explicit microbial dynamics. The results of the simulations are compared for a reaction network that considers the secondary reactions versus one that ignores them (reactions I-7 to I-18 in Wang and Van Cappellen (1996)).

### 3. Results and discussion

#### 3.1. Pore scale simulations

Using our simple approximation to microbial respiration, simulations show the existence of preferential flow paths (Fig. 1). However, pore scale heterogeneity in biomass and substrate concentrations is small. Steady state distributions of acetate and biomass in solution computed from Eqs. (3)–(5) for the Sherwood aquifer setting show virtually no variation at the pore scale, as diffusion is a dominant process at this scale (Fig. 1; the quartile ranges of concentrations in the fluid phase, determined from simulation results interpolated onto a regular 0.46 μm by 0.35 μm grid, are 0.48–0.49 μM and 0.22–0.24 mg<sub>dw</sub> m<sup>-3</sup>, respectively). Acetate concentrations have reached the point where its uptake is limiting growth. Sorption/desorption occurs at sufficient rate to cause a near-equilibrium distribution between mobile and immobile

biomass, with the majority of the cells (>98%) being surface-associated.

To elucidate the conditions under which either the flow regime or reaction dynamics vary significantly at the grain scale, the parameterization of the baseline simulations was altered systematically. A ten-fold increase in the substrate production rate  $R_{prod}$  from  $10^{-8}$  to  $10^{-7}$  mol m $^{-3}$  s $^{-1}$  or a spatially uneven distribution of acetate production (e.g. production via breakdown of particulate organic matter, modeled as a source term associated with grain surfaces or constrained to a single quadrant of the domain) did not lead to patchy concentration fields. Substantial spatial variations in substrate and biomass concentrations are seen only when  $R_{prod}$  is increased by two orders of magnitude. Under this condition, quartile ranges for the aquifer are 0.46–0.63  $\mu$ M acetate and 0.023–0.029 g $_{dw}$ m $^{-3}$  biomass, respectively. Similarly, increasing the pressure gradient by an order of magnitude in our simulations did not lead to spatial heterogeneity, because the advective timescale ( $L$ /average velocity) exceeds that of diffusion ( $L^2/D$ ) at the scale of the domain ( $L$ ), and even more so at the pore level. For heterogeneity in substrate and biomass concentrations to become significant in our simulations, advective or reactive processes must occur on a shorter timescale than diffusion as observed by Raje and Kapoor (2000) and Gramling et al. (2002) in soil columns at a high Péclet number. The reactive timescale (estimated by the ratio of the average substrate concentration to the acetate consumption rate) of the simulations becomes shorter than the diffusional timescale when substrate production rates are increased by 2 orders of magnitude. This indicates that heterogeneity can potentially become dominant in environmental conditions that promote fast reactions, albeit at rates that likely exceeds microbial respiration.

### 3.2. Macroscopic redox zonation

All implementations of the contaminant plume reaction network are subject to the same rate laws characterizing the phenol breakdown and the resulting acetate and H $_2$  production, with the exception of the simulations in which the microbial populations are accounted for explicitly. With only a fraction of the inflowing phenol being degraded, and due to the similarity in rate laws in all simulations, the phenol plume (Fig. 2A) is nearly identical in shape and magnitude in all simulations, matching the observations closely (see comparison of model results to the measured well profile in Fig. 2C). However, because of the dependency of aerobic phenol breakdown and denitrification (P1 and P2 in Table 1) on O $_2$  and NO $_3^-$  concentrations, the competition for oxidants by introduction of secondary reactions leads to a drop in the aerobic respiration rate. Taking into account the use of O $_2$  in the oxidation of reduced inorganics leads to an ~40% lower phenol breakdown over the course of the 47 years studied compared to the baseline network alone, and the contribution of aerobic to total phenol degradation is reduced from ~48 to ~14% (Table 3).

Rate laws of acetate and total H $_2$  consumption via methanogenesis and the reduction of sulfate and iron and manganese oxides are identical for the above networks, and both acetate and H $_2$  contours roughly follow the plume outline for the reaction networks analyzed (Fig. 2A, B). Following the implementation in Watson et al. (2005), H $_2$  respiration is only

modeled in suboxic and anoxic conditions. This is consistent with the absence of any overlap between O $_2$  and H $_2$  in field measurements (Thornton et al., 2001b), as well as in our model simulations. Therefore, in contrast to the impact of secondary reactions on phenol degradation, little to no effect from secondary reactions on H $_2$  dynamics is observed. The impact of the further addition of carbonate mineral precipitation on DIC concentrations is small, so that the DIC plume in Fig. 2B is representative for all reaction networks.

Redox sensitive products of the organic matter breakdown reactions reveal differences between reaction networks. Simulations only accounting for primary reactions match measured Mn(II) levels fairly well (Thornton et al., 2001b; not shown), but lead to dissolved iron concentrations exceeding those observed (Table 3; simulated Fe $^{2+}$  levels at well BH60 after 47 years are approximately 3 fold higher than the measured values shown in Fig. 3 of Thornton et al. (2001b)). In all reaction networks investigated, the total concentration of iron oxides was virtually unaffected by the different reaction networks because of the large pool size. In addition, the total reduced iron pool (Fe $^{2+}$  + >Fe + FeS + FeCO $_3$ ; where >Fe represents surface adsorbed iron) varies by less than a factor of 3 (Table 3); however, the speciation of the iron can differ substantially. Taking into account secondary reactions results in an increase of Fe $^{2+}$  by ~10% and an ~75% decrease in the amount of FeS. The inclusion of mineral precipitation reactions tends to lower the Fe $^{2+}$ , >Fe, and FeS pools since the iron is precipitated as FeCO $_3$ , which constitutes the largest sink for reduced iron (~60%).

As for the contaminant plume, inclusion of secondary reactions in sediment simulations results in the lowering of the importance of the aerobic degradation of organic matter from ~32% to 11% (Table 3). The effect of network complexity on iron speciation has a greater impact in the marine sediment than in the contaminant plume setting. For example, iron oxide levels are ~3.5 times more prevalent considering the full reaction network than in simulations not accounting for the secondary reactions. Inclusion of secondary reactions also impacts reduced iron pools, doubling the integrated Fe $^{2+}$  concentrations while FeS decreases by ~39%. In comparison, addition of the secondary reactions in the contaminant plume results in a 10% increase in Fe $^{2+}$  levels. Overall, total reduced iron levels are increased by ~12% upon accounting for secondary reactions (Table 3).

Aside from these highlighted differences in iron pools, our results show that changes in the reaction network have relatively little impact on pool sizes for most chemicals, but can affect reaction pathways. This is consistent with the results of Hunter et al. (1998) who assessed the importance of secondary reactions in simulations of a pristine aquifer contaminated by a landfill leachate. They found that the concentrations of organic matter were unaffected by the inclusion of secondary reactions, but that consistent with the effects on aerobic oxidation of phenol, the competition for O $_2$  by secondary reactions altered the pathways of organic matter decomposition. Thullner et al. (2005) determined that manganese reduction was completely controlled by secondary reactions in a coastal marine setting, although it was more pronounced than the impact of secondary reactions on iron cycling presented here. These results highlight the fact that not taking into account all of the relevant reactions can lead to

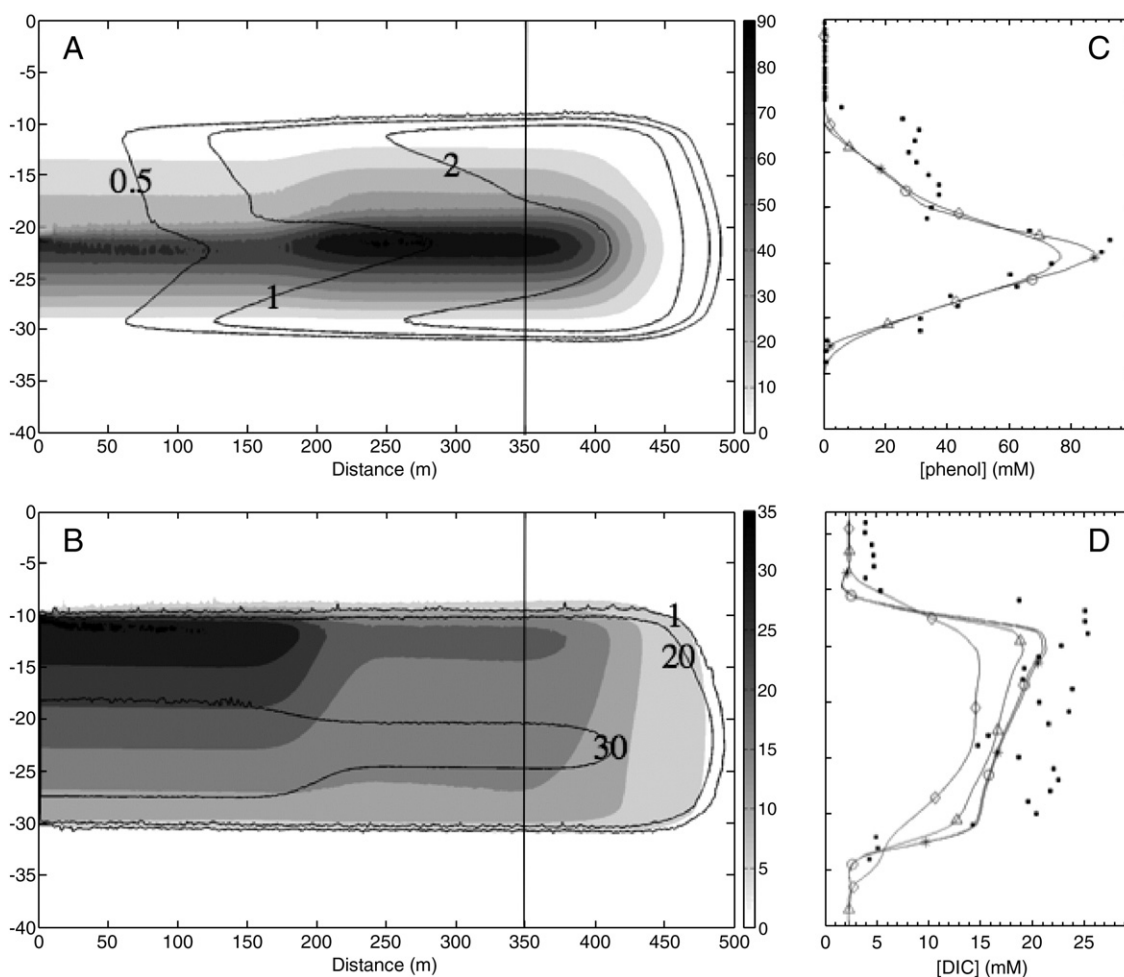


**Fig. 2.** (A) Contaminant plume after 47 years. Shaded regions in panels (A) and (B) show phenol and DIC in mM, respectively, while the contour lines denote acetate (mM, A) and  $H_2$  concentrations (nM, B), respectively. The vertical bar indicates the position of a well for which panels (C) and (D) show a comparison of the measurements represented by filled circles (dots; Thornton et al., 2001b) and the model results (lines). For panels (C) and (D), open circles denote reaction network P,E; asterisks denote P,E,S; triangles denote P,E,S,M; and diamonds denote P,E,S,M,B.

improper conclusions about the importance of biodegradation pathways. They also show that the specific environment plays a role in the extent of the effect of secondary reactions. Inclusion of secondary reactions has a greater effect in the sediment environment, where redox interfaces are more prevalent and  $O_2$  consumption via secondary reactions plays a greater role than in the contaminant plume simulation.

### 3.3. Plume scale microbial distributions

The addition of explicit descriptions of phenol fermenting, phenol respiring, and hydrogen respiring microbial populations lead to little spatial variability in modeled cell densities. Phenol fermenters were estimated to be present predominantly within the plume at  $\sim 8 \times 10^6$  cells  $ml^{-1}$ , while computed phenol respiring organisms were found near the plume edge in similar concentrations;  $H_2$  oxidizers were similar in spatial extent to the phenol fermenters but present at higher concentrations of  $\sim 2 \times 10^7$  cells  $ml^{-1}$  (not shown). Inclusion of microbial populations leads to geochemical distribution patterns consistent with the observations (Fig. 2). Our parameterization slightly

underpredicted dissolved inorganic carbon production (Fig. 2D), concurring with a higher estimate of acetate than the non-biotic reaction networks which in part is also caused by a slightly higher phenol breakdown. While total iron levels are consistent with non-biotic simulations, there is an approximate doubling of the  $FeCO_3$  and increased dissimilatory iron reduction (Table 3).

Our simulations show relatively little spatial variation in total bacterial numbers (not shown). Consistent with our findings, Thullner et al. (2005), who introduced microbial groups into a reactive transport model describing a marine sediment, determined that bacteria were distributed homogeneously. Similarly, Dale et al. (2006), who accounted for bacterial groups and energetic limitation in coastal sediment, also found little variation in bacterial biomass concentrations over time. Our simulations also indicate that the regulation of biomass levels depends on nitrogen limitations and thermodynamic constraints (Fig. 3). This finding in our carbon rich environment contrasts starkly with dissolved organic carbon limited microbial populations in a groundwater setting described by Lensing et al. (1994). Simulations that did not take into account nitrogen

**Table 3**

Concentrations ( $\text{mol m}^{-1}$ ) and reaction rates ( $\text{mol m}^{-1} \text{s}^{-1}$ ) for the contaminant plume simulations under different reaction network formulations integrated over space, as indicated by the  $\int_x$ . Percentages of total reduced iron for each species are given in parentheses. For organic matter oxidation by oxygen, the percentage of total organic matter degradation is given in parentheses.

	<sup>a</sup> Contaminant plume				<sup>b</sup> Sediment	
	P,E	P,E,S	<sup>c</sup> P,E,S,M	P,E,S,M,B	Full – S	Full
$\int_x \text{FeOx}$	$3.4 \times 10^6$	$3.4 \times 10^6$	$3.4 \times 10^6$	$3.4 \times 10^6$	$2.71 \times 10^1$	$9.43 \times 10^1$
$\int_x \text{Fe}^{2+}$	$8.1 \times 10^2$ (21.4)	$9.0 \times 10^2$ (19.2)	$2.2 \times 10^2$ (10.0)	$1.8 \times 10^2$ (4.3)	$1.0 \times 10^0$	$2.4 \times 10^0$
$\int_x > \text{Fe}$	$2.8 \times 10^3$ (73.2)	$3.7 \times 10^3$ (79.6)	$6.2 \times 10^2$ (27.6)	$8.3 \times 10^2$ (19.4)	$3.68 \times 10^1$	$8.44 \times 10^1$
$\int_x \text{FeCO}_3$	–	–	$1.4 \times 10^3$ (60.0)	$3.2 \times 10^3$ (74.9)	0	$2.35 \times 10^2$
$\int_x \text{FeS}$	$2.1 \times 10^2$ (5.4)	$5.8 \times 10^1$ (1.2)	$5.4 \times 10^1$ (2.4)	$6.0 \times 10^1$ (1.4)	$6.80 \times 10^2$	$4.15 \times 10^2$
$\int_x \text{Fe}^{\text{red}}$	$3.8 \times 10^3$	$4.7 \times 10^3$	$2.2 \times 10^3$	$4.3 \times 10^3$	$7.48 \times 10^2$	$8.38 \times 10^2$
<sup>d</sup> $\int_x R_{\text{resp}}(\text{O}_2)$	$1.0 \times 10^{-6}$ (47.7)	$2.0 \times 10^{-7}$ (14.4)	$2.1 \times 10^{-7}$ (15.0)	$6.8 \times 10^{-7}$ (35.5)	$5.9 \times 10^{-6}$ (32.2)	$2.1 \times 10^{-6}$ (11.3)
<sup>e</sup> $\int_x R_{\text{resp}}(\text{FeOx})$	$9.1 \times 10^{-7}$	$9.1 \times 10^{-7}$	$9.1 \times 10^{-7}$	$2.3 \times 10^{-6}$	$5.8 \times 10^{-7}$	$3.8 \times 10^{-6}$

<sup>a</sup> “P,E” refers to the baseline simulation, “S” to inclusion of secondary reactions, “M” to mineral precipitation/dissolution reactions, and “B” to explicit descriptions of microbial functional groups. See Table 1 for the reactions part of each set.

<sup>b</sup> “Full” refers to the complete set of reactions in Wang and Van Cappellen (1996), “Full – S” to the removal of the secondary reactions.

<sup>c</sup> Note that, following the work of Watson et al. (2005), precipitation/dissolution of FeS is in the primary reaction network “P,E” even before additional precipitation/dissolution reactions are added in “P,E,S,M”.

<sup>d</sup> Organic matter degradation coupled to oxygen.

<sup>e</sup> Organic matter degradation coupled to iron hydroxides.

limitation demonstrated unrestrained bacterial growth due to the virtually unlimited availability of phenol, while simulations with no thermodynamic constraints resulted in lower  $\text{H}_2$  concentration throughout the domain (not shown). Nitrogen is abundant within approximately the first 75 m of the domain and does not inhibit microbial growth, while the remainder of the plume is nitrogen limited (Fig. 3B). An analysis of bacterial growth dynamics within nitrogen limited regions shows a steady state existence of the bacterial groups with cell death and nitrogen release being balanced by subsequent growth. Abundant energy is available for bacteria respiring  $\text{O}_2$  and  $\text{NO}_3^-$ , but for organisms fermenting high molecular weight organic compounds,  $F_{\text{thd}}$  varies from  $\sim 0.6$  to 1 with the strongest thermodynamic constraints in areas of the plume with the highest acetate concentrations (Fig. 3A). The bacterial group respiring  $\text{H}_2$  shows an  $F_{\text{thd}}$  term that varies between  $\sim 0.5$  and 0.7 (Fig. 3B), suggesting that energetic constraints contribute to shaping *in situ* microbial activity.

#### 4. Conclusions

This study, focusing on conditions in a sandy aquifer, assesses two aspects that may pose limitations to reactive transport modeling: pore scale variability and the comprehensiveness of the (micro-)biogeochemical processes considered.

First, simulations of flow and concentration fields subject to (idealized) biogeochemical dynamics suggest little spatial variability in substrate and biomass distributions at the grain scale, at least under conditions that do not favor the formation of biofilms. Second, results from simulations using different reaction networks show that a relatively simple reaction network can provide an accurate prediction of the observed distribution of dissolved substances in a contaminant plume. However, depending on complexity of the reaction network used, distinct differences can exist in individual process rates affecting these pools. Simulations of the breakdown of organics in groundwater highlights the importance of reoxidation reactions in settings characterized by strong redox gradients

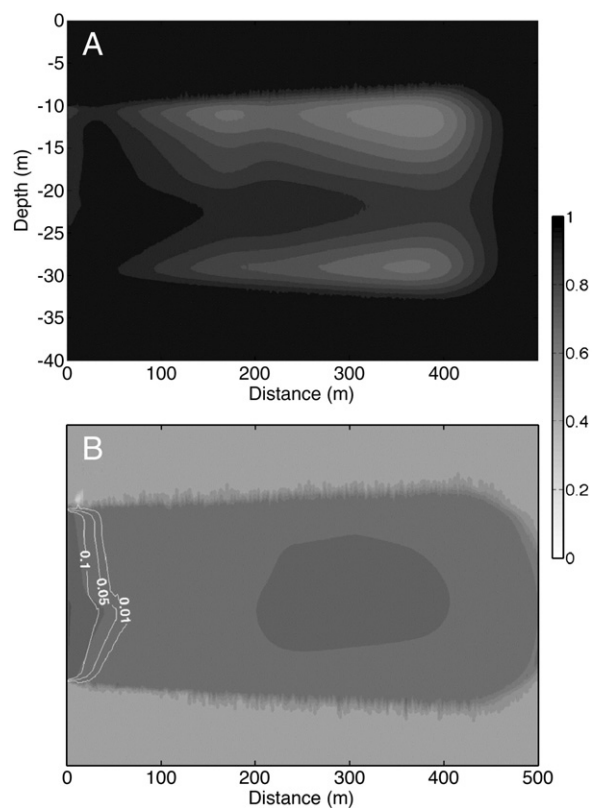


**Fig. 3.** Bacterial nitrogen and thermodynamic limitations for phenol fermenting (panel A) and  $\text{H}_2$  oxidizing bacteria (panel B). Filled regions indicate the value of the thermodynamic constraint, computed as  $\sum R_i F_{\text{thd},i} / \sum R_i$ , where  $R_i$  denotes the relevant kinetic reaction rates,  $B^* F_{\text{kin}}$  (P3 and P4 in panel A, P5, P6, P7, and P8 in panel B) and  $F_{\text{thd},i}$  the corresponding thermodynamic factors. The contours (panel B) represent the concentration of available ammonium (mM), indicating that in most of the plume,  $\text{NH}_4^+$  requirements are met only via recycling of biomass.

over a large part of the model domain; a finding supported by the assessment of their impact on process dynamics in coastal marine surface sediments. This is notable, because while concentration fields only denote snapshots compared to transient model simulations, they are typically used for model validation. Our results emphasize the need for comparison of modeled process dynamics with measured rates, which are difficult to obtain and hence are not readily available.

Consistent with the results of Wang and Papenguth (2001), we found that a description of subsurface processes may not always require an explicit representation of microbial biomass, particularly in settings characterized by minimal microbial activity. However, accounting for growth of microbes and associated reaction rates requires going beyond implementation of a kinetic substrate dependency of biomass alone. Notably, inclusion of nitrogen limitations appeared necessary in a setting fueled by carbohydrates to avoid excessive microbial growth due to abundant C-substrate. The need to account for a range of feedback mechanisms between microbial activity and environmental conditions suggests that understanding microbial requirements (which may extend well beyond the factors and chemical substances encompassed in current reactive transport models) may be central to quantify controls on bioremediation in the field.

## Acknowledgments

We thank Harlan Miller III for his help with the pore scale simulations and Philippe Van Cappellen for use of STEADYSED. This work was supported by the Office of Science of the United States Department of Energy (DE-FG02-05ER25676), and it benefited substantially from the constructive criticism and insightful comments of 3 anonymous reviewers.

## References

- Boudart, M., 1976. Consistency between kinetics and thermodynamics. *J. Phys. Chem.* 80, 2869–2870.
- Boudreau, B.P., 1996. A method-of-lines code for carbon and nutrient diagenesis in aquatic sediments. *Comput. Geosci.* 22 (5), 479–496.
- Bradford, S.A., Yates, S.R., Bettahar, M., Simunek, J., 2002. Physical factors affecting the transport and fate of colloids in saturated porous media. *Water Resour. Res.* 38, 1327–1339.
- Bratbak, G., Dundas, I., 1984. Bacterial dry-matter content and biomass estimations. *Appl. Environ. Microbiol.* 48, 755–757.
- Brown, P.N., Byrne, G.D., Hindmarsh, A.C., 1989. VODE: a variable-coefficient ODE solver. *SIAM J. Sci. Comput.* 10, 1038–1051.
- Coppola, A., Comegna, V., Basile, A., Lamaddalena, N., Severino, G., 2009. Darcian preferential water flow and solute transport through bimodal porous systems: Experiments and modeling. *J. Contam. Hydrol.* 104, 74–83.
- Cygan, R.T., Stevens, C.T., Puls, R.W., Yabusaki, S.B., Wauchope, R.D., McGrath, C.J., Curtis, G.P., Siegel, M.D., Veblen, L.A., Turner, D.R., 2007. Research activities at U.S. government agencies in subsurface reactive transport modeling. *Vadose Zone J.* 6, 805–822.
- Dale, A.W., Regnier, P., Van Cappellen, P., 2006. Bioenergetic controls on anaerobic oxidation of methane (AOM) in coastal marine sediments: a theoretical analysis. *Am. J. Sci.* 306, 246–294.
- Davison, W., Fones, G.R., Grime, G.W., 1997. Dissolved metals in surface sediment and a microbial mat at 100- $\mu\text{m}$  resolution. *Nature* 387, 885–888.
- Esteve-Núñez, A., Rothermich, M., Sharma, M., Lovley, D.R., 2005. Growth of Geobacter sulfurreducens under nutrient-limiting conditions in continuous culture. *Environ. Microbiol.* 7, 641–648.
- Ginn, T.R., Wood, B.D., Nelson, K.E., Scheibe, T.D., Murphy, E.M., Clement, T.P., 2002. Processes in microbial transport in the natural subsurface. *Adv. Water Res.* 25, 1017–1042.
- Gramling, C.M., Harvey, C.F., Meigs, L.C., 2002. Reactive transport in porous media: a comparison of model prediction with laboratory visualization. *Environ. Sci. Technol.* 36, 2508–2514.
- Hassanizadeh, S.M., 1995. On the transient non-Fickian dispersion theory. *Trans. Porous Media.* 23, 107–124.
- Hunter, K.S., Wang, Y., Van Cappellen, P., 1998. Kinetic modeling of microbially-driven redox chemistry in subsurface environments: coupling transport, microbial metabolism and geochemistry. *J. Hydrol.* 209, 53–58.
- Jakobsen, R., Albrechtsen, H.J., Rasmussen, M., Bay, H., Bjerg, P.L., Christensen, T.H., 1998.  $\text{H}_2$  concentrations in a landfill leachate plume (Grinsted, Denmark): in situ energetics of terminal electron acceptor processes. *Environ. Sci. Technol.* 32, 2142–2148.
- Jakobsen, R., Postma, D., 1999. Redox zoning, rates of sulfate reduction and interactions with Fe-reduction and methanogenesis in a shallow sandy aquifer, Romo, Denmark. *Geochim. Cosmochim. Acta* 63, 137–151.
- Jakobsen, R., 2007. Redox microniches in groundwater: a model study on the geometric and kinetic conditions required for concomitant Fe oxide reduction, sulfate reduction, and methanogenesis. *Water Resour. Res.* 43 (12), W12S12.
- Jakobsen, R., Cold, L., 2007. Geochemistry at the sulfate reduction–methanogenesis transition zone in an anoxic aquifer – a partial equilibrium interpretation using 2D reactive transport modeling. *Geochim. Cosmochim. Acta* 71, 1949–1966.
- Jin, Q., Bethke, C.M., 2003. A new rate law describing microbial respiration. *Appl. Environ. Microbiol.* 69, 2340–2348.
- Jin, Q.S., Bethke, C.M., 2005. Predicting the rate of microbial respiration in geochemical environments. *Geochim. Cosmochim. Acta* 69 (5), 1133–1143.
- King, E.L., Tuncay, K., Ortoleva, P., Meile, C., 2009. In silico microbial metabolism of Geobacter sulfurreducens and its representation in reactive transport models. *Appl. Environ. Microbiol.* 75, 83–92. doi:10.1128/AEM.01799-08.
- Lensing, H.J., Vogt, M., Herrling, B., 1994. Modeling of biologically mediated redox processes in the subsurface. *J. Hydrol.* 159, 125–143.
- Levy, M., Berkowitz, B., 2003. Measurement and analysis of non-Fickian dispersion in heterogeneous porous media. *J. Contam. Hydrol.* 64, 203–226.
- Li, L., Peters, C.A., Celia, M.A., 2006. Upscaling geochemical reaction rates using pore-scale network modeling. *Adv. Water Res.* 29, 1351–1370.
- Li, L., Steefel, C.I., Yang, L., 2008. Scale dependence of mineral dissolution rates within single pores and fractures. *Geochim. Cosmochim. Acta* 72, 360–377.
- Lovley, D.R., Goodwin, S., 1988. Hydrogen concentrations as an indicator of the predominant terminal electron-accepting reactions in aquatic sediments. *Geochim. Cosmochim. Acta* 52, 2993–3003.
- Mayer, K.U., Benner, S.G., Frind, E.O., Thornton, S.F., Lerner, D.N., 2001. Reactive transport modeling of processes controlling the distribution and natural attenuation of phenolic compounds in a deep sandstone aquifer. *J. Contam. Hydrol.* 53, 341–368.
- McNab, W.W., Narasimhan, T.N., 1994. Modeling reactive transport of organic-compounds in groundwater using a partial redox disequilibrium approach. *Water Resour. Res.* 30, 2619–2635.
- McNab, W.W., Narasimhan, T.N., 1995. Reactive transport of petroleum hydrocarbon constituents in a shallow aquifer – modeling geochemical interactions between organic and inorganic species. *Water Resour. Res.* 31, 2027–2033.
- Meile, C., Tuncay, K., 2006. Scale dependence of reaction rates in porous media. *Adv. Water Res.* 29, 62–71.
- Miller, C.T., Christakos, G., Imhoff, P.T., McBride, J.F., Pedit, J.A., Trangenstein, J.A., 1998. Multiphase flow and transport modeling in heterogeneous porous media: challenges and approaches. *Adv. Water Res.* 21, 77–120.
- Murphy, E.M., Ginn, T.R., 2000. Modeling microbial processes in porous media. *Hydrogeol. J.* 9, 142–158.
- Narsilio, G.A., Buzzi, O., Fityus, S., Yun, T.S., Smith, D.W., 2009. Upscaling of Navier–Stokes equations in porous media: Theoretical, numerical and experimental approach. *Comput. Geotech.* 36 (7), 1200–1206.
- Pett-Ridge, J., Firestone, M.K., 2005. Redox fluctuation structures microbial communities in a wet tropical soil. *Appl. Environ. Microbiol.* 71, 6998–7007.
- Raje, D.S., Kapoor, V., 2000. Experimental study of bimolecular reaction kinetics in porous media. *Environ. Sci. Technol.* 34, 1234–1239.
- Reddy, J., 1993. An introduction to the finite element method 2nd ed. McGraw-Hill, Inc, New York. 684p.
- Saiers, J.E., Hornberger, G.M., 1996. Migration of Cs-137 through quartz sand: experimental results and modeling approaches. *J. Contam. Hydrol.* 22 (3–4), 255–270.
- Scheidegger, A., 1961. General theory of dispersion in porous media. *J. Geophys. Res.* 66, 3273–3278.
- Scott, J.B.T., Barker, R.D., 2005. Characterization of sandstone by electrical spectroscopy for stratigraphical and hydrogeological investigations. *Q. J. Eng. Geol. Hydrogeol.* 38, 143–154.
- Seeliger, S., Cord-Ruwisch, R., Schink, B., 1998. A periplasmic and extracellular c-type cytochrome of Geobacter sulfurreducens acts as a ferric iron

- reductase and as an electron carrier to other acceptors or to partner bacteria. *J. Bacteriol.* 180 (14), 3686–3691.
- Sochaczewski, L., Stockdale, A., Davison, W., Tych, W., Zhang, H., 2008. A three-dimensional reactive transport model for sediments, incorporating microniches. *Environ. Chem.* 5 (3), 218–225.
- Soetaert, K., Herman, P.M.J., Middelburg, J.J., 1996. A model of early diagenetic processes from the shelf to abyssal depths. *Geochim. Cosmochim. Acta* 60 (6), 1019–1040.
- Spiteri, C., Slomp, C., Tuncay, K., Meile, C., 2008. Modeling biogeochemical processes in subterranean estuaries: the effect of flow dynamics and redox conditions on submarine groundwater discharge of nutrients. *Water Resour. Res.* 44. doi:10.1029/2007WR006071.
- Steeffel, C., MacQuarrie, K., 1996. Approaches to modeling of reactive transport in porous media. In: Lichtner, P., Steefel, C., Oelkers, E. (Eds.), *Reactive Transport in Porous Media*, Vol. 34. Mineralogical Society of America, pp. 83–130.
- Steeffel, C.L., DePaolo, D.J., Lichtner, P.C., 2005. Reactive transport modeling: an essential tool and a new research approach for the Earth sciences. *Earth Planet. Sci. Lett.* 240, 539–558.
- Stumm, W., Morgan, J.J., 1996. *Aquatic Chemistry*. John Wiley & Sons, Inc. 1022p.
- Suchomel, B.J., Chen, B.M., Allen, M.B., 1998. Network model of flow, transport and biofilm effects in porous media. *Transp. Porous Media.* 30 (10), 1–23.
- Szecsody, J.E., Zachara, J.M., Chilakapati, A., Jardine, P.M., Ferreny, A.S., 1998. Importance of flow and particle-scale heterogeneity on Coll/III EDTA reactive transport. *J. Hydrol.* 209, 112–136.
- Tadanier, C.J., Eick, M.J., 2002. Formulating the charge-distribution multisite surface complexation model using FITEQL. *Soil Sci. Soc. Am. J.* 66, 1505–1517.
- Thullner, M., Van Cappellen, P., Regnier, P., 2005. Modeling the impact of microbial activity on redox dynamics in porous media. *Geochim. Cosmochim. Acta* 69, 5005–5019.
- Thornton, S.F., Lerner, D.N., Banwart, S.A., 2001a. Assessing the natural attenuation of organic contaminants in aquifers using plume-scale electron and carbon balances: model development with analysis of uncertainty and parameter sensitivity. *J. Contam. Hydrol.* 53, 199–232.
- Thornton, S.F., Quigley, S., Spence, M.J., Banwart, S.A., Bottrell, S., Lerner, D.N., 2001b. Processes controlling the distribution and natural attenuation of dissolved phenolic compounds in a deep sandstone aquifer. *J. Contam. Hydrol.* 53, 233–267.
- Van Cappellen, P., Wang, Y., 1996. Cycling of iron and manganese in surface sediments: a general theory for the coupled transport and reaction of carbon, oxygen, nitrogen, sulfur, iron and manganese. *Am. J. Sci.* 296, 197–243.
- Wang, Y., Van Cappellen, P., 1996. A multicomponent reactive transport model of early diagenesis: application to redox cycling in coastal marine sediments. *Geochim. Cosmochim. Acta* 60, 2993–3014.
- Wang, Y., Papenguth, H.W., 2001. Kinetic modeling of microbially-driven redox chemistry of radionuclides in subsurface environments: coupling transport, microbial metabolism and geochemistry. *J. Contam. Hydrol.* 47, 297–309.
- Watson, I.A., Oswald, S.E., Banwart, S.A., Crouch, R.S., Thornton, S.F., 2005. Modeling the dynamics of fermentation and respiratory processes in a groundwater plume of phenolic contaminants interpreted from laboratory–to field-scale. *Environ. Sci. Technol.* 39, 8829–8839.
- Williams, G.M., Pickup, R.W., Thornton, S.F., Lerner, D.N., Mallinson, H.E.H., Moore, Y., White, C., 2001. Biogeochemical characterization of a coal tar distillate plume. *J. Contam. Hydrol.* 53, 175–197.
- Wood, B.D., Radakovich, K., Golfier, F., 2007. Effective reaction at a fluid–solid interface: applications to biotransformation in porous media. *Adv. Water Res.* 30, 1630–1647.
- Zhang, D., Zhang, R., Chen, S., Soll, W.E., 2000. Pore scale study of flow in porous media: scale dependency, REV, and statistical REV. *Geophys. Res. Lett.* 27, 1195–1198.